

Vibrational mode and collision energy effects on reaction of H_2CO^+ with C_2H_2 : Charge state competition and the role of Franck-Condon factors in endoergic charge transfer

Jianbo Liu, Brian Van Devener, and Scott L. Anderson^{a)}
 Department of Chemistry, University of Utah, Salt Lake City, Utah 84112

(Received 28 September 2005; accepted 4 October 2005; published online 28 November 2005)

The effects of collision energy (E_{col}) and six different H_2CO^+ vibrational states on the title reaction have been studied over the center-of-mass E_{col} range from 0.1 to 2.6 eV, including measurements of product ion recoil velocity distributions. *Ab initio* and Rice-Ramsperger-Kassel-Marcus calculations were used to examine the properties of complexes and transition states that might be important in mediating the reaction. Reaction is largely direct, despite the presence of multiple deep wells on the potential surface. Five product channels are observed, with a total reaction cross section at the collision limit. The competition among the major H_2^+ transfer, hydrogen transfer, and proton transfer channels is strongly affected by E_{col} and H_2CO^+ vibrational excitation, providing insight into the factors that control competition and charge state “unmixing” during product separation. One of the more interesting results is that endoergic charge transfer appears to be controlled by Franck-Condon factors, implying that it occurs at large inter-reactant separations, contrary to the expectation that endoergic reactions should require intimate collisions to drive the necessary energy conversion.

© 2005 American Institute of Physics. [DOI: 10.1063/1.2128670]

I. INTRODUCTION

We report a study of the effects of collision energy (E_{col}) and H_2CO^+ vibrational excitation on the reaction of $\text{H}_2\text{CO}^+ + \text{C}_2\text{H}_2$. Both H_2CO^+ and acetylene are important in astrochemical environments,^{1–4} where nonequilibrium conditions make vibrational effects important. A selected ion flow tube (SIFT) study of the $\text{H}_2\text{CO}^+ + \text{C}_2\text{H}_2$ reaction was recently reported by Francis *et al.*,⁵ in which they reported rates for proton transfer (branching ratio=25%) and H_2^+ transfer (75%) at thermal energies (background prevented measurements of other channels). Here, integral cross sections and product ion velocity distributions were measured for the reaction of mode-selective, excited H_2CO^+ with C_2H_2 over the center-of-mass collision energy (E_{col}) range from 0.1 to 2.6 eV. Five product ions are observed, corresponding to charge transfer (CT), proton transfer (PT), hydrogen transfer (HT), H_2^+ transfer (HPT), and hydrogen elimination (HE) from an intermediate complex. The E_{col} and vibrational state dependence of the cross sections gives information about inter-channel competition and insight into the effects of energy, angular momentum, and different types of nuclear motion.

One interesting feature of the $\text{H}_2\text{CO}^+ + \text{C}_2\text{H}_2$ system is that there are two pairs of product channels differing only in which fragment carries the charge. The first pair is $\text{H}_2\text{CO} + \text{C}_2\text{H}_2^+$ (CT) vs $\text{H}_2\text{CO}^+ + \text{C}_2\text{H}_2$ [nonreactive (NR) scattering]. We are able to measure the cross section for nonreactive scattering, using time-of-flight to discriminate this channel from unscattered primary ions. The second pair is $\text{HCO}^+ + \text{C}_2\text{H}_3$ (HT) vs $\text{HCO} + \text{C}_2\text{H}_3^+$ (PT). Competition within each

pair depends on the factors controlling charge state mixing, and competition between the pairs and with other channels provides insight about the points on the reaction path where the charge states begin to “unmix.”

One of the more interesting observations is that the vibrational mode dependence of the CT cross section is exactly that expected for CT controlled by the Franck-Condon factors connecting the reactant states to energetically accessible product states. The Franck-Condon control is expected for exoergic CT occurring at long inter-reactant separations, but for the endoergic CT channel here, the usual picture is that “hard” collisions are required to drive the necessary conversion of collision energy to internal energy. Careful analysis of the nonreactive scattering cross section is also consistent with substantial energy conversion at large separations.

A common feature of an ion-molecule reaction is the existence of intermediate complexes on the potential energy surface that can mediate reaction, especially at low collision energies.^{6–11} Typically, two types of complexes are of interest. Strongly bound covalent complexes can mediate complicated rearrangements, and may be required for certain product channels. Weakly bound electrostatic complexes typically form readily, and may increase the probability for reaction or for isomerization to covalent complexes. Quantum chemistry calculations were used to locate these complexes and the transition states connecting the complexes to each other and to various products. The Rice-Ramsperger-Kassel-Marcus (RRKM) theory was then used to estimate the statistical behavior expected for the system, for comparison with experimental observation. The measured product ion velocity distributions, as well as product branching, provide a good test of the importance of statistical mechanisms.

^{a)}Author to whom correspondence should be addressed. Electronic mail: anderson@chem.utah.edu

II. EXPERIMENTAL AND COMPUTATIONAL DETAILS

The guided ion-beam tandem mass spectrometer used in this study has been described previously,^{12–15} along with the operation, calibration, and data analysis procedures. The H_2CO precursor was generated from paraformaldehyde (Aldrich 95%) mixed with anhydrous MgSO_4 (Merck) at 60 °C.¹⁶ The resulting H_2CO was carried into a pulsed molecular beam valve using a flow of helium at ~ 1 atm, giving a H_2CO concentration of $\sim 5\%$.¹⁷ H_2CO^+ can be generated in selected vibrational states by resonance-enhanced multiphoton ionization (REMPI) through the $^1A_2(3p_x)$ Rydberg state,¹⁸ and here we examine the reactions of H_2CO^+ in its ground state, or with one quantum in the following modes: ν_2^+ (CO stretch, 0.208 eV), ν_3^+ (CH_2 scissors, 0.143 eV), ν_4^+ (CH_2 out-of-plane bend, 0.114 eV), ν_5^+ (CH_2 asymmetric stretch, 0.337 eV), and ν_6^+ (CH_2 rock, 0.101 eV). The ions were generated inside a short radio-frequency (rf) quadrupole ion guide which focused the ions into a quadrupole mass filter. Mass-selected ions were collected and collimated by a set of lenses equipped with variable apertures and a gating electrode. The combination of controlled collection radius and time gating allows us to produce a mass-selected beam with a narrow kinetic energy spread ($\Delta E \approx 0.1$ eV).

The mass-, vibrational state-, and kinetic energy-selected primary beam was injected into a system of eight-pole rf ion guides.¹⁹ In the first segment of the guide, ions were passed through a 10-cm-long scattering cell, containing acetylene at 4×10^{-5} Torr. The C_2H_2 (Matheson, 99%) and C_2D_2 (Cambridge Isotope Laboratory, $>99\%$ D atom) reactants were purified by passage through a dry ice/acetone trap, and the inlet valve was kept at about 70 °C to avoid freezing acetylene in the valve orifice. Product ions and unreacted primary ions were collected by the ion guide, passed into a second, longer guide segment for time-of-flight (TOF) analysis, then mass analyzed and counted. Integral cross sections were calculated from the ratio of reactant and product ion intensities, and the calibrated target gas pressure-length product. TOF was used to measure the reactant ion velocity distribution (and thus the E_{col} distribution) at each nominal E_{col} , and also to measure the product ion axial velocity distributions discussed below.

For each reactant state we cycled through the series of E_{col} values several times, in order to minimize the systematic error from drifting potentials, etc. As a check on reproducibility, we measured the cross sections for the ground state at the beginning and end of each complete experimental run. Finally, the entire set of experiments was repeated several times. We estimate that the uncertainty in the absolute scale of the ground-state cross section is $\sim 10\%$, primarily from the uncertainties in the target pressure and the collection efficiency for slow product ions. More importantly, based on the reproducibility of the cross-section measurements, we estimate that the relative error (e.g., uncertainty in comparing data for different vibrational states or E_{col}) is less than 10%.

To map out the reaction coordinate, electronic structure calculations were performed at the B3LYP/6-311++G** level of theory, using GAUSSIAN03.²⁰ The vibrational frequen-

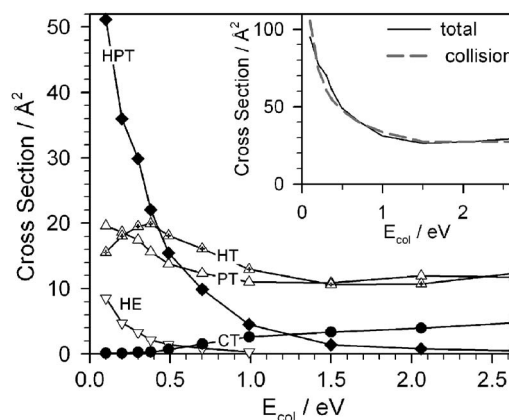


FIG. 1. Cross sections for the reaction of ground-state H_2CO^+ with C_2H_2 . Also shown are the total reaction cross section and the estimated collision cross section.

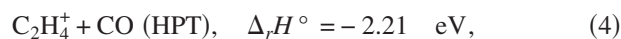
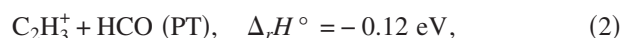
cies and zero-point energies were scaled by factors of 0.9613 and 0.9804, respectively.²¹ All transition states (TSs) were verified to be first-order saddle points by frequency calculations. When necessary, intrinsic reaction coordinate (IRC) calculations were used to determine which minima are connected by each particular TS. The RRKM rate and density-of-states calculations were done with the program of Zhu and Hase,²² using its direct state count option and frequencies and energetics from the B3LYP/6-311++G** calculations.

III. RESULTS AND ANALYSIS

A. Integral cross sections

The integral cross sections for the reaction of ground-state H_2CO^+ with C_2H_2 are shown in Fig. 1 over the center-of-mass (c.m.) E_{col} range from 0.1 to 2.6 eV. The inset to Fig. 1 shows the experimental total cross section (σ_{total} = sum of individual cross section) and an estimate of the collision cross section (σ_{col}), taken as greater of the ion-induced dipole capture cross section (σ_{capture}) and the hard-sphere cross section ($\sigma_{\text{hard sphere}}$). $\sigma_{\text{hard sphere}}$ was calculated from the orientation-averaged contact radius of H_2CO^+ and C_2H_2 assuming covalent radii for each atom, and exceeds σ_{capture} for $E_{\text{col}} \geq 1.5$ eV. Within experimental error, σ_{total} is equal to σ_{col} i.e., the total reaction efficiency ($\sigma_{\text{total}}/\sigma_{\text{col}}$) is unity at all collision energies.

The $\text{H}_2\text{CO}^+ + \text{C}_2\text{H}_2$ isotope combination was used in most experiments. Product ions are observed at m/z 26, 27, 28, 29, and 55, corresponding to C_2H_2^+ , C_2H_3^+ , C_2H_4^+ , HCO^+ , and CH_2CHCO^+ . The energetics (298 K) for the following reaction channels are calculated based on the thermochemical data tabulated by Lias *et al.*²³ and Lias:²⁴



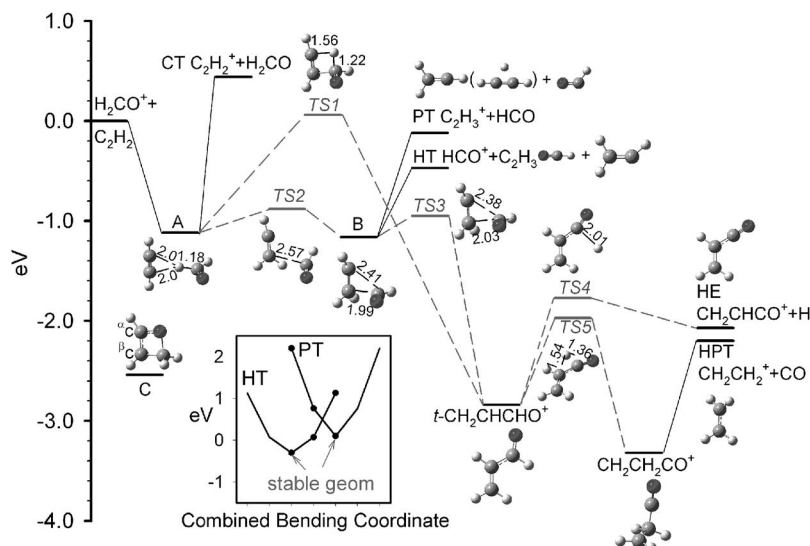


FIG. 2. Schematic reaction coordinate for $\text{H}_2\text{CO}^+ + \text{C}_2\text{H}_2$. The energies are derived from a combination of experimental and B3LYP/6-311++G** values, the latter including zero-point energies. The bond distances are shown in Angstroms. The inset shows the potential curves for the HT and PT products, where the x axis is the combined bending coordinate that carries the system between the equilibrium geometries of the two charge states. The points are calculated, and the curves are just to guide the eyes.



To look for possible atom scrambling during reaction and to distinguish which reactant supplies the H eliminated in the HE channel, we also measured the integral cross sections for reaction with C_2D_2 . In this case the HPT channel cannot be monitored because of interference from the H_2CO^+ beam, and the only product masses were m/z 28 ($d_2\text{-C}_2\text{H}_2^+$), 29 ($d_2\text{-C}_2\text{H}_3^+$ and HCO^+), and 57 ($d_2\text{-CH}_2\text{CHCO}^+$). As far as can be determined, there is no H/D scrambling. In particular, the H eliminated in the HE channel always comes from the H_2CO^+ reactant.

For many systems where PT is exothermic, it tends to dominate, even when there are more energetically favorable channels.^{7,10,11,25} In this system, the HPT channel dominates by a large margin for low E_{col} . The HPT : PT branching in the thermal energy SIFT measurements of Francis *et al.*⁵ is consistent with our measurements at the lowest E_{col} , although they were unable to measure the other three product channels for experimental reasons. HPT is strongly suppressed by collision energy, dropping to less than 5% of σ_{total} for $E_{\text{col}}=2.0$ eV. The PT and HT channels are simply the two lowest energy electronic states (i.e., charge states) of the $[\text{C}_2\text{H}_3 + \text{HCO}]^+$ products, with HT being more energetically favorable. At high E_{col} the two channels have nearly identical, E_{col} -independent cross sections. As E_{col} decreases, both σ_{HT} and σ_{PT} increase, with the more exoergic HT channel growing more rapidly. For $E_{\text{col}} < \sim 0.4$ eV, the growth of σ_{PT} slows and σ_{HT} decreases. This E_{col} dependence suggests the competition of the HT/PT pair with the HPT and HE channels.

Despite the fact that HE is considerably more energetically favorable than PT or HT, the HE cross section is significant only at the lowest energies, declining to near zero at E_{col} above 0.5 eV. This behavior is consistent with the fact that forming the most stable product structure (CH_2CHCO^+) requires C–C bond formation and H migration prior to H elimination, suggesting that HE may require mediation by a long-lived complex. What is surprising in that case is the absence of D elimination in reaction with C_2D_2 , which one might expect to result from H/D scrambling in the complex.

The absence of D elimination also rules out the formation of the $\text{HC}\equiv\text{C-CH}_2\text{O}^+$ isomer of the HE product ion.^{26,27}

CT has an appearance energy around 0.3 eV, compared to the 0.42 eV thermodynamic threshold. The shift simply reflects various experimental broadening factors, and the simulation/fitting of the $\sigma_{\text{CT}}(E_{\text{col}})$ data to extract the true energy dependence is discussed below.

B. Computational results

The computational results for $\text{H}_2\text{CO}^+ + \text{C}_2\text{H}_2$ are summarized in Fig. 2 and Table I, where energetics are reported as $\Delta_r H^\circ$ (298 K) to allow a comparison with the experimental results compiled by Lias *et al.*²³ and Lias.²⁴ Figure 2 indicates our calculated lowest energy reaction coordinate, with experimental energetics for products and B3LYP/6-311++G** values for complexes and TSs. Note that the PT product ion C_2H_3^+ can have either classical or hydrogen-bridged

TABLE I. Experimental and calculated $\Delta_r H^\circ$ (eV) relative to the reactants $\text{H}_2\text{CO}^+ + \text{C}_2\text{H}_2$.

Reaction energetics	$\Delta_r H^\circ$ (298 K)	
	B3LYP/6-311++G** ^a	Experimental ^b
$\rightarrow \text{C}_2\text{H}_2^+ + \text{H}_2\text{CO}$	0.64	0.42
$\rightarrow \text{C}_2\text{H}_3^+ + \text{HCO}$	-0.10	-0.12
$\rightarrow \text{C}_2\text{H}_4^+ + \text{CO}$	-2.07	-2.21
$\rightarrow \text{HCO}^+ + \text{C}_2\text{H}_3$	-0.30	-0.47
$\rightarrow \text{CH}_2\text{CHCO}^+ + \text{H}$	-1.91	-2.07
Complex A	-1.12	...
Complex B	-1.16	...
<i>trans</i> - $\text{CH}_2\text{CHCHO}^+$	-2.84	...
$\text{CH}_2\text{CH}_2\text{CO}^+$	-3.32	...
TS1	0.06	...
TS2	-0.88	...
TS3	-0.95	...
TS4	-1.77	...
TS5	-1.97	...

^aZero-point energy calculated at B3LYP/6-311++G** was scaled by 0.9804.

^bExperimental values of $\Delta_r H^\circ$ (298 K) are taken from Refs. 23 and 24.

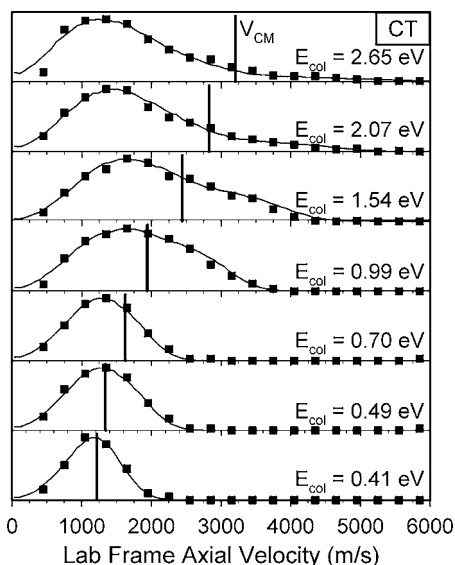


FIG. 3. Axial recoil velocity distributions for the CT product ions. Solid symbols: Experimental data. Solid line: Simulation based on the osculating complex model. Heavy vertical line: $\langle V_{c.m.} \rangle$.

structures, which are isoenergetic at the B3LYP/6-311++G^{*} level of theory. Two weakly bound complexes (A and B) and two covalently bound complexes (*trans*-CH₂CHCHO⁺ and CH₂CH₂CO⁺) were found. We attempted to locate the TSs connecting the complexes to each other and to the products, as shown in Fig. 2. There are other covalently bound species with C₃H₄O⁺ stoichiometry (e.g., CH₃CHCO⁺, CHCHCHOH⁺, CH₂CCHOH⁺, cyclo-CH₂CHCHO⁺, cyclo-CH₂CH₂CO⁺, and cyclopropanone cation) that have been studied computationally by Li and Baer,²⁸ Francis *et al.*,⁵ McKee and Radom,²⁹ Turecek *et al.*,^{30,31} and Bouchoux.³² These complexes are not included in the reaction coordinate here, because their formation involves either activation barriers inconsistent with the experimental energy dependence or rearrangements that are inconsistent with the observed absence of H/D scrambling and the very short reaction time scale (see below). The Li and Baer study focused on the reaction coordinate for the unimolecular decomposition of CH₂CHCHO⁺, but did not explore much of the reaction coordinate shown in Fig. 2. Our results are consistent with their HF/6-31G^{*} and B3LYP/6-31G^{*} results, with the exception that our TS3 has a slightly different structure and lower energy than the analogous TS in their study.

Complex A is a reactant-like electrostatic pseudo-hydrogen-bonded complex, with the H₂CO⁺ hydrogen equidistant at 2.0 Å from the two acetylene carbon atoms. The binding energy of complex A is 1.12 eV with respect to the reactants, and because no rearrangement is required, a significant activation barrier to its formation is unlikely. The Mulliken charge analysis and natural population analysis³³ (NBO) both indicate that in complex A the charge is >50% transferred to the acetylene moiety, i.e., complex A is product-like from the perspective of CT. Complex B is a product-like electrostatic complex, where one of the formaldehyde hydrogen atoms has been transferred to acetylene, leaving HCO bonded to C₂H₃ with binding energies of 1.04

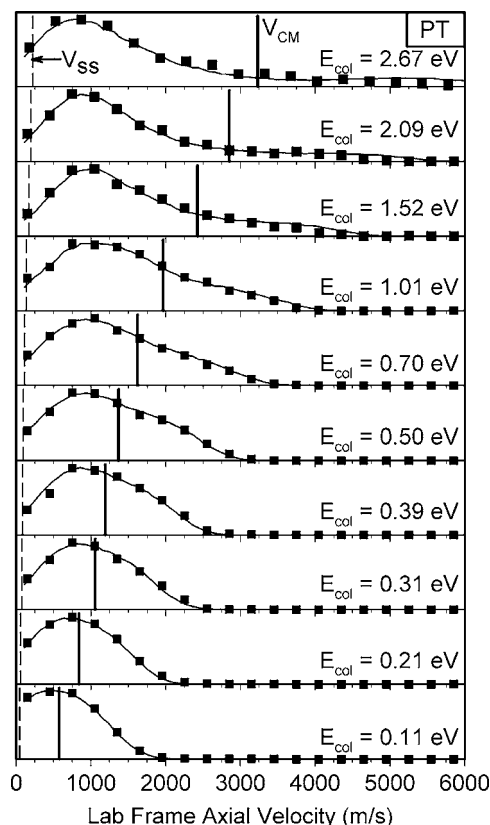


FIG. 4. Axial recoil velocity distributions for the PT product ions. Solid symbols: Experimental data. Solid line: Simulation based on the osculating complex model. Heavy vertical line: $\langle V_{c.m.} \rangle$. Dashed line: Spectator-stripping-limit product velocity.

and 0.69 eV with respect to PT and HT products, respectively. Complex B can form from complex A via TS2 with an energy barrier of 0.24 eV relative to complex A. The charge is roughly equally split between the C₂H₃ and HCO moieties in complex B, and presumably it can decay either to HT or PT products. Forming the covalently bound complexes, *trans*-CH₂CHCHO⁺ and CH₂CH₂CO⁺, requires C–C bond formation and hydrogen migration. We have been able to locate transition states (TS3 and TS5) that allow the formation of *trans*-CH₂CHCHO⁺ via isomerization of complex B and CH₂CH₂CO⁺ via hydrogen atom transfer from *trans*-CH₂CHCHO⁺, respectively, with activation energies well below the reactant energy. Note that *trans*-CH₂CHCHO⁺ can alternatively form from complex A via TS1, but because TS1 is 0.06 eV above the reactant energy and relatively tight, this pathway is not expected to be important. *Trans*-CH₂CHCHO⁺ can eliminate H from the aldehyde carbon atom via TS4,³⁴ forming the most stable HE product isomer CH₂CHCO⁺.³⁵ The distonic ion CH₂CH₂CO⁺ can lose CO to generate HPT products, and in principle can also lose H to generate HE products. The latter path is not shown, based on collision-induced dissociation (CID) studies of Traeger *et al.*,³⁴ which showed that *trans*-CH₂CHCHO⁺ mostly loses H, while CH₂CH₂CO⁺ mostly loses CO.

Figure 2 shows the minimum energy reaction paths suggested by the calculations. The CT channel may be complex A mediated; however, complex formation is certainly not required. The lowest energy routes to HT and PT products

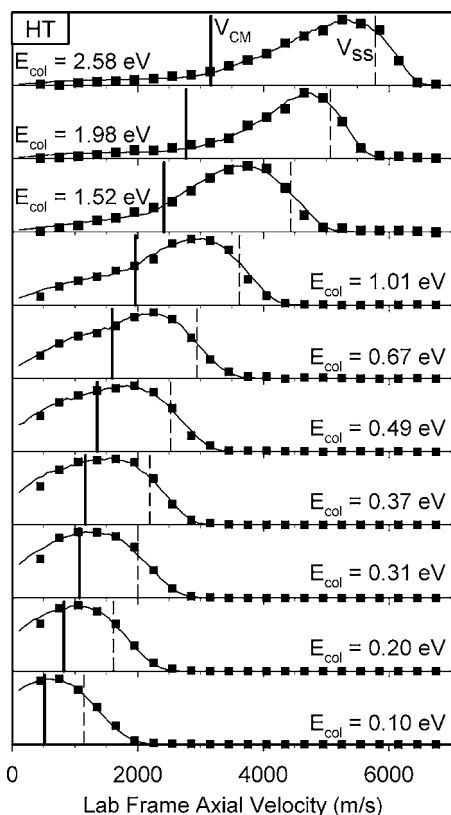


FIG. 5. Axial recoil velocity distributions for the HT product ions. Solid symbols: Experimental data. Solid line: Simulation based on the oscillating complex model. Heavy vertical line: $\langle V_{c.m.} \rangle$. Dashed line: Spectator-stripping-limit product velocity.

are reactants \rightarrow complex $A \rightarrow$ TS2 \rightarrow complex $B \rightarrow$ PT or HT products. The structures for C_2H_3 and $C_2H_3^+$, and for HCO and HCO^+ are quite different, thus we might expect that the PT/HT branching will be influenced by the geometry of the products as they separate. In complex B , the C_2H_3 and HCO moieties both have bent geometries similar to those of the neutral species, and the charge is equally partitioned, thus the complex itself does not appear to favor either HT or PT. In the absence of dynamical effects, branching would just be determined by the number of accessible vibronic levels belonging to the two charge states.³⁶

The lowest energy route found to HE products is reactants \rightarrow complex $A \rightarrow$ TS2 \rightarrow complex $B \rightarrow$ TS3 \rightarrow *trans*- CH_2CHCHO^+ \rightarrow TS4 \rightarrow HE. We note that in Li and Baer's study,²⁸ a different transition state analogous to TS3 was reported for the isomerization between complex B and *trans*- CH_2CHCHO^+ . This transition state is ~ 0.25 eV higher than TS3; moreover, both frequency analysis and an IRC calculation suggest that this TS is more likely a transition state for hydrogen atom transfer within the C_2H_3 moiety, and not for the C-C bond formation required to produce *trans*- CH_2CHCHO^+ .

The lowest energy pathway found to HPT products also passes through the *trans*- CH_2CHCHO^+ complex: reactants \rightarrow complex $A \rightarrow$ TS2 \rightarrow complex $B \rightarrow$ TS3 \rightarrow *trans*- CH_2CHCHO^+ \rightarrow TS5 \rightarrow $CH_2CH_2CO^+ \rightarrow C_2H_4^+ + CO$. In addition to a mechanism similar to this, Francis *et al.*⁵ proposed another complex-mediated mechanism for HPT as follows. A

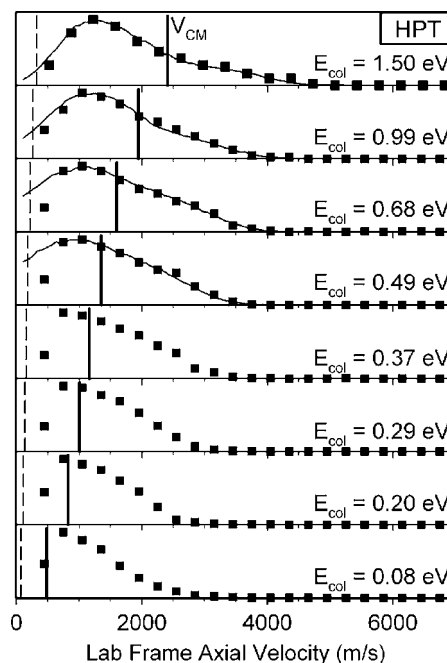


FIG. 6. Axial recoil velocity distributions for the HPT product ions. Solid symbols: Experimental data. Solid line: Simulation based on the oscillating complex model. Heavy vertical line: $\langle V_{c.m.} \rangle$.

covalent complex C as shown in Fig. 2, with a four membered ${}^{\alpha}C^{\beta}CCO$ ring, was proposed to form from the reactants, then undergo a ${}^{\alpha}C$ to ${}^{\beta}C$ hydrogen shift. The ${}^{\alpha}C$ - ${}^{\beta}C$ bond of acetylene and the O-C bond of H_2CO^+ then dissociate, leading to $C_2H_4^+$ that contains carbon atoms originating from both H_2CO^+ and acetylene. This mechanism was not verified by isotope labeling, and we tend to discount it for several reasons. The formation of complex C is unlikely to be efficient enough to contribute significantly to the large HPT cross section, because both the acetylene and H_2CO^+ reactants require large distortions, and the collision would have to be in a narrow range of reactant orientation. More importantly, the TS for the ${}^{\alpha}C$ - ${}^{\beta}C$ hydrogen shift is quite tight and is only -0.05 eV below the reactants (in their results), suggesting that any complex C that forms would primarily decay back to the reactants through an orbiting TS. Finally, we have done a RRKM estimate of the lifetime for complex C , and found that it is substantially longer than the time scale observed experimentally.

C. Recoil velocity distributions

TOF data were collected for product ions at a series of E_{col} values and for each vibrational state. Velocity distributions for the HE channel were not analyzed because the heavy-ion-light-neutral kinematics preclude extracting useful information. The laboratory-frame v_{axial} distributions for CT, PT, HT, and HPT product ions are given in Figs. 3, 4, 5, and 6, respectively. Also shown as solid vertical lines in each figure are the velocities of the CM frame with respect to the laboratory frame, $\langle V_{c.m.} \rangle$, averaged over the distributions of the reactant ion and target velocities. For comparison, the velocities expected from the spectator-stripping mechanism

(V_{SS}) (Ref. 37) are indicated with dashed vertical lines in Figs. 4–6 for PT, HT, and HPT product ions.

Axial velocity (v_{axial}) distributions are simply the projection of the full velocity distributions on the ion guide axis. Because our experiment is axially symmetric, the laboratory-frame v_{axial} distributions can be approximately converted to the c.m. frame simply by subtracting $\langle V_{c.m.} \rangle$. The raw laboratory frame v_{axial} distributions, thus, provide several types of useful dynamical insight. The partitioning of available energy into product recoil is reflected in the displacement of v_{axial} distribution features relative to $\langle V_{c.m.} \rangle$. Furthermore, if the reaction is mediated by a complex with lifetime (τ_{col}) greater than its rotational period (τ_{rot}), the resulting v_{axial} distribution must be symmetric about $\langle V_{c.m.} \rangle$. Conversely, an asymmetric v_{axial} distribution is a clear sign that the reaction is direct (i.e., not complex-mediated), and also reveals the dominant scattering mechanism (i.e., forward versus backward scattering). It is important to note, however, that a symmetric distribution is not proof of a complex-mediated mechanism, particularly for low E_{col} where asymmetries may be masked by experimental broadening if the recoil velocity is small enough.

Another experimental problem is that product ions that are strongly backscattered in the c.m. frame may have negative laboratory velocities. To collect such ions, the ion lens at the upstream end of the ion guide is biased positive relative to the guide potential, reflecting these ions back toward the detector. The reflected ions appear at long flight times, corresponding to low but positive laboratory velocities. In addition, the slowest ions are most likely to have their velocities distorted by inhomogeneous surface potentials, and these distortions are exacerbated by the singular TOF-to-velocity Jacobian. In analyzing the velocity distributions, data points at velocities below ~ 450 m/s, where the distortions are most problematic, are ignored.

In the limit of high E_{col} , product angular distributions are expected to depend primarily on the distributions of the impact parameter (b) leading to each product channel, with small b collisions leading to rebounding products and large b collisions to stripping. The v_{axial} distributions for all channels are strongly asymmetric with respect to $\langle V_{c.m.} \rangle$ at high E_{col} , indicating direct reaction mechanisms. The distributions for HT products are peaked forward of $\langle V_{c.m.} \rangle$, while the distributions for CT, PT, and HPT are backward-peaked. Here, “forward” and “backward” are defined as product ions with axial velocities faster or slower, respectively, than $\langle V_{c.m.} \rangle$. With this definition, the sense of forward and backward is opposite for channels where the charge is transferred (PT, CT, and HPT), compared with those where it is not (HT). In this system, therefore, all major channels at high E_{col} are dominated by stripping-type mechanisms, i.e., by collisions at large b leading to the transfer of e^- , H^+ , H , or H_2^+ , without the large angular deflection of the collision partners. The presence of tails in the v_{axial} distributions well into the backward (HT) or forward (CT, PT, and HPT) directions indicates that small impact-parameter (rebounding) collisions also contribute to each channel to varying degrees.

The overall dominance of stripping-type dynamics is not surprising. The fact that σ_{total} is equal to σ_{col} implies that the

reaction must be efficient at all b , and large b collisions occur with higher probability than small b collisions. What is somewhat surprising is that all channels are dominated by large b collisions, despite the fact that the individual high E_{col} cross sections vary considerably in magnitude. The HPT channel (Fig. 6) does have higher intensity in the forward scattered tail of the v_{axial} distribution, relative to CT, PT, and HT. In the absence of v_{axial} information, the fact that $\sigma_{HPT} < 0.05\sigma_{total}$ for $E_{col} \geq 1$ eV might be taken as evidence that HPT occurs primarily in small b collisions. The v_{axial} distribution shows that while small b collisions are somewhat more important than in the other major channels, large b collisions still dominate HPT, and the small cross section simply reflects low reaction efficiency at all impact parameters.

As E_{col} is reduced, the peaks in the v_{axial} distributions for all channels shift toward $\langle V_{c.m.} \rangle$, reflecting the decreasing amount of energy available to drive recoil. Note that $\langle V_{c.m.} \rangle$ decreases to only ~ 500 m/s at the lowest E_{col} , only slightly greater than the minimum velocity (~ 450 m/s) where we feel that the measurements are reliable. As a consequence, we cannot determine whether or not the v_{axial} distributions become forward-backward symmetric at the lowest E_{col} . It is clear, however, that the distributions for the HT, PT, and HPT channels are asymmetric for $E_{col} \geq 0.2$ eV, i.e., the mechanisms are clearly direct at high E_{col} , and possibly at low E_{col} as well.

For CT, the distributions appear forward-backward symmetric for $E_{col} \leq 0.49$ eV. To a large extent the apparent symmetry probably reflects the fact that these energies are just above the threshold, thus there is little energy available to drive recoil. Because of the experimental broadening from the ion beam and target velocity distributions, the true recoil velocity distributions would have to be highly asymmetric to result in resolvable asymmetry in the experimental distributions.

To correct for the experimental broadening, we simulated and fitted the experimental distributions. The HPT results at low E_{col} were not analyzed because the shape of the experimental distributions suggests that much of the product distribution may be back-scattered in the laboratory frame, where we cannot measure it. Our fitting program and procedures have been described previously.¹² In short, a model recoil velocity distribution is assumed, then run through a Monte Carlo-based simulation of the experiment that includes all the broadening factors. The model distribution, based on the osculating complex model,³⁸ is adjusted until the simulation and experiment are consistent. In the osculating complex model, a short-lived collision complex is assumed to form, with rotational angular momentum (and period τ_{rot}) determined by the orbital angular momentum of the collision. The collision complex is assumed to decay to products with a lifetime $\tau_{complex}$ and a recoil energy distribution $P(E_{recoil})$. $P(E_{recoil})$ is assumed to be a Gaussian distribution parametrized in terms of the available energy (E_{avail}) in each product channel. The most important aspect of the experimental distributions—the degree of forward-backward symmetry—depends only on the ratio τ_{col}/τ_{rot} and by varying τ_{col}/τ_{rot} the model can treat both complex-mediated and

TABLE II. Product ion velocity distribution fit results for $\text{H}_2\text{CO}^+ + \text{C}_2\text{H}_2$.

E_{col} (eV)	$\langle E_{\text{avail}} \rangle$ (eV) ^a	$\langle E_{\text{recoil}} \rangle$ (eV)	$\langle E_{\text{recoil}} \rangle / \langle E_{\text{avail}} \rangle$ (%)	τ_{col} (ps)	$\tau_{\text{fly-by}}$ (ps) ^b
C_2H_2^+ (CT)					
0.41	0.06	0.04	66	>1.00	0.21
0.49	0.13	0.08	60	1.00	0.19
0.70	0.31	0.14	45	0.70	0.16
0.99	0.59	0.27	46	0.50	0.14
1.54	1.14	0.46	40	0.21	0.11
2.07	1.67	0.76	46	0.10	0.09
2.65	2.25	1.18	52	<0.10	0.08
C_2H_3^+ (PT)					
0.11	0.27	0.12	44	>1.00	0.41
0.21	0.36	0.13	36	1.00	0.39
0.31	0.47	0.18	38	0.56	0.24
0.39	0.55	0.21	38	0.46	0.22
0.50	0.66	0.27	41	0.44	0.19
0.70	0.85	0.36	42	0.26	0.16
1.01	1.17	0.52	44	0.18	0.13
1.52	1.68	0.81	48	0.12	0.11
2.09	2.25	1.31	58	0.10	0.09
2.67	2.83	1.84	65	<0.10	0.08
HCO^+ (HT)					
0.10	0.61	0.22	36	>1.00	0.42
0.20	0.71	0.26	37	0.83	0.30
0.31	0.82	0.31	37	0.56	0.24
0.37	0.88	0.35	40	0.46	0.22
0.49	1.00	0.40	40	0.40	0.20
0.67	1.18	0.42	36	0.26	0.16
1.01	1.52	0.64	42	0.16	0.13
1.52	2.03	0.84	41	0.10	0.11
1.98	2.48	1.41	57	<0.10	0.09
2.58	3.09	1.66	54	<0.10	0.08
C_2H_4^+ (HPT)					
0.49	2.74	0.48	17	0.50	0.20
0.68	2.93	0.55	18	0.23	0.16
0.99	3.24	0.59	18	0.18	0.14
1.50	3.75	0.65	17	0.13	0.11

^a $\langle \rangle$ = mean value.^b $\tau_{\text{fly-by}}$ defined as the time for undeflected reactants to travel a relative distance of 5.0 Å.

direct scatterings. To put τ_{col} on an absolute basis, τ_{rot} can be estimated from the moment of inertia and angular momentum of the complex, the latter estimated from the magnitude of the cross section and E_{col} . Assuming a complex like *A* in Fig. 2, forming with a cross section at the collision limit, τ_{rot} drops smoothly from ~ 1.3 ps at $E_{\text{col}}=0.1$ eV to 0.5 ps at $E_{\text{col}}=2.6$ eV. The solid curves shown in Figs. 3–6 are the fits, and the numerical results are summarized in Table II.

As shown in Table II, τ_{col} for CT, PT, HT, and HPT drops rapidly with increasing E_{col} , reflecting the increasingly asymmetric v_{axial} distributions. As an indication of the collision time that might be expected in the limit of a direct mechanism, Table II also gives $\tau_{\text{fly-by}}$, taken as the time required for the reactants to move a relative distance of 5 Å. For the HPT channel, τ_{col} is comparable to $\tau_{\text{fly-by}}$ at all collision energies. For CT, PT, and HT, τ_{col} exceeds $\tau_{\text{fly-by}}$ at low E_{col} , but becomes comparable by $E_{\text{col}} \sim 1.0$ eV. Clearly, any complexes that form are short-lived, consistent with the

absence of H/D exchange in reaction with C_2D_2 . It should be noted that the osculating complex model assumes that the degree of forward-backward symmetry results entirely from rotation of a collision complex. This assumption becomes increasingly dubious with decreasing τ_{col} and as discussed above, the shapes of the distributions at high E_{col} are expected to depend mostly on the distribution of impact parameters contributing to each product channel.

Table II also includes the estimates of the average energy partitioned into recoil $\langle E_{\text{recoil}} \rangle$ extracted from the fits. For PT and HPT, the $\langle E_{\text{recoil}} \rangle$ values extracted should be lower limits on the true values, because ions with low laboratory velocities (i.e., high c.m. velocities) are excluded from the fits. The table gives both $\langle E_{\text{avail}} \rangle$ and $\langle E_{\text{recoil}} \rangle$ and the fraction of E_{avail} going into recoil ($\langle E_{\text{recoil}} \rangle / \langle E_{\text{avail}} \rangle$). For all channels, there is a net conversion of E_{col} into the internal energy of the products, i.e., E_{recoil} is less than E_{col} even for the exoergic channels. For all the channels except HPT, both $\langle E_{\text{recoil}} \rangle$ and

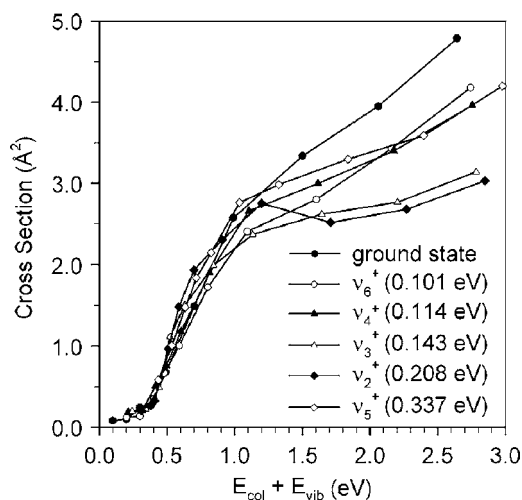


FIG. 7. CT cross sections plotted against $E_{\text{col}}+E_{\text{vib}}$ for the reaction of $\text{H}_2\text{CO}^+(\nu^+)$ with C_2H_2 .

$\langle E_{\text{recoil}} \rangle / \langle E_{\text{avail}} \rangle$ increase with increasing E_{col} , indicating that faster collisions are more likely to retain E_{col} as a product translational energy. For the highly exoergic HPT channel, the $\langle E_{\text{recoil}} \rangle / \langle E_{\text{avail}} \rangle$ fractions are small and nearly constant, indicating that the reaction exoergicity is mostly partitioned to internal energy.

Velocity distributions were also measured for the reaction of vibrationally excited H_2CO^+ . These are not shown, as they are qualitatively quite similar to those for ground-state reactants. The similarity reflects the fact that recoil velocity distributions are largely determined by kinematics and by the energy available to drive recoil, which is not changed much

by one quantum of reactant vibrational excitation. The exception is the CT v_{axial} distributions, which become more backward peaked, with higher $\langle E_{\text{recoil}} \rangle$, upon H_2CO^+ vibrational excitation. The effects are only significant for $E_{\text{col}} \leq \sim 1$ eV, and some of the increase in $\langle E_{\text{recoil}} \rangle$ can be attributed to the fact that in this E_{col} range, the added vibrational energy significantly increases E_{avail} for this endoergic channel. The increased backward peaking reflects the vibrational enhancement of the CT cross section at low E_{col} , and demonstrates that the enhancement results mostly from increased CT probability in large b collisions. Because such collisions tend to convert a smaller fraction of E_{col} to product internal energy, this change in the reactive b distribution also tends to increase $\langle E_{\text{recoil}} \rangle$.

D. Vibrational effects

Figure 7 shows σ_{CT} plotted versus $(E_{\text{col}}+E_{\text{vib}})$, for the reaction of H_2CO^+ in the six vibrational states examined. Rotational energy (E_{rot}) was omitted because it is independent of vibrational state and collision energy and small compared to $E_{\text{col}}+E_{\text{vib}}$. Note, however, that E_{rot} is included in the simulations of v_{axial} distributions (above) and of the threshold behavior (below). It can be seen that σ_{CT} scales like E_{total} from the appearance energy up to ~ 1 eV, but there are mode-specific vibrational effects at higher energies, suggesting a change in mechanism. Figure 8 shows the effects of vibrational excitation on all product channels, as well as σ_{total} , for three different ranges of E_{col} . The effects are given as ratios of cross sections for the reaction of a particular state $\sigma(\nu^+)$ to the cross section for the reaction of the ground state

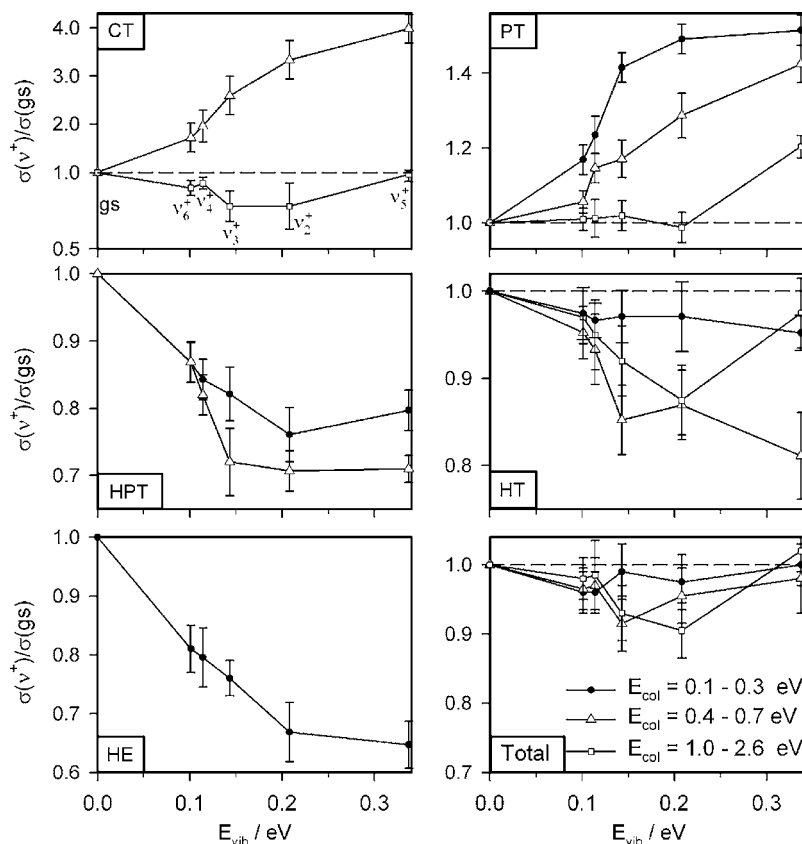


FIG. 8. Vibrational enhancement/inhibition factors vs E_{vib} , for different E_{col} ranges, for the reactions of $\text{H}_2\text{CO}^++\text{C}_2\text{H}_2$.

$\sigma(\text{gs})$ plotted against E_{vib} . Each E_{vib} point corresponds to one of the six states studied, as indicated by labels in the top left frame. To reduce statistical uncertainty in the ratios, the data for the indicated ranges of E_{col} have been averaged. The error bars were estimated from variations between multiple data sets. Effects are seen at all E_{col} , with the largest effects generally at the lowest E_{col} , except for the HT channel, where vibration has large effects at all energies.

IV. DISCUSSION

A. Reactions at high E_{col}

The significant product channels at high collision energies ($E_{\text{col}} \geq 1$ eV) are CT, PT, HT, and HPT, and the product ion v_{axial} distributions indicate that all four channels are dominated by direct stripping-type reaction mechanisms. We first consider CT. At high E_{col} the v_{axial} distributions for all the six H_2CO^+ vibrational states are strongly peaked in the backward direction (small angle scattering). Because the collision time is short at high E_{col} (Table II), the shape of the velocity distribution is expected to depend most strongly on the distribution of impact parameters leading to CT. The measured distributions suggest that CT occurs over a range of impact parameters ranging from zero (the forward-scattered tail) to moderately large (the backward peak). The breadth of the distributions, and the fact that they peak at laboratory velocities well above zero, indicate that there is considerable momentum transfer, consistent with the requirement for 0.42 eV of translational-to-internal energy conversion to drive CT. The factors controlling CT at high E_{col} are discussed in the section below on vibrational effects.

The competition among the PT, HT, and HPT channels provides an interesting window on the dynamics controlling branching in the major channels. At the highest E_{col} , HPT is negligible and PT and HT account for $>80\%$ of σ_{total} . HCO^+ produced by CID would add to the apparent HT product signal, complicating the analysis of PT/HT branching for E_{col} above the 1.09 eV H_2CO^+ dissociation energy. Several observations suggest that this contribution is negligible. We have studied the CID of H_2CO^+ in collisions with Ne and Xe,¹⁵ and the cross sections at 2.1 eV are small compared to σ_{HT} 0.3 and 1.4 Å² for Ne and Xe, respectively. Moreover, no CID is observed in H_2CO^+ collisions with CD_4 (Ref. 8) and OCS ,⁷ where as in the present system, CID competes with other reactions. Finally, we note that HCO^+ produced by CID is predominantly backscattered,¹⁵ whereas in the present system there is little backscattered HT signal at high E_{col} (Fig. 5).

The HT and PT channels are simply the two lowest electronic states (i.e., charge states) of the $[\text{C}_2\text{H}_3+\text{HCO}]^+$ products. The actual atom transfer event must take place in a geometry where the reactants are interacting intimately, and in such geometries (e.g., complexes *A* and *B* and TS2) the charge is calculated to be roughly equally partitioned between the two collision partners, i.e., the charge states are mixed. The branching between HT and PT must, therefore, be determined at some point during the separation of the $[\text{C}_2\text{H}_3+\text{HCO}]^+$ products. The asymptotic energetics favor HT, and in the absence of dynamical effects, the PT/HT ratio

should be proportional to the number of accessible rovibrational states in each channel. On this basis, the PT/HT branching ratio should be near unity for collision energies large compared to the HT-PT energy difference, decreasing as the collision energy is decreased. This simple picture is consistent with the experiment PT/HT branching for E_{col} down to ~ 0.5 eV, but at lower E_{col} the trend reverses as competition with HPT and HE becomes important. This interesting behavior provides insight into the processes controlling charge state branching, and will be discussed in the next section.

From a dynamical perspective, the HPT channel is perhaps the most interesting and hardest to understand. The HPT signal is significant in the high E_{col} range; however, it is clear that this signal simply represents a small remnant of what is primarily a low E_{col} channel; therefore its mechanism will be considered further in the next section. The main point regarding HPT at high E_{col} is that it clearly is direct, with rather short collision times (Fig. 6 and Table II), despite the need to transfer two atoms to different carbon centers.

B. Reactions at low E_{col}

1. Is complex mediation important?

At high E_{col} , all reactions are clearly direct with collision times comparable to $\tau_{\text{fly-by}}$. For low E_{col} , the apparently symmetric v_{axial} distributions for all channels raise the possibility that the mechanism becomes complex-mediated. To evaluate whether the complexes and transition states identified in our *ab initio* calculations can account for the experimental observations, we used the RRKM program of Zhu and Hase²² to calculate the lifetimes and decay branching of all the complexes shown in Fig. 2 except complex *C*, including all the decomposition channels indicated by lines in that figure. For the decay of complex *A* to reactants and to CT products, of complex *B* to PT and to HT products, and of $\text{CH}_2\text{CH}_2\text{CO}^+$ to HPT products, there is no reason to expect energy barriers in excess of the asymptote, thus we have assumed orbiting transition states.³⁹ For these calculations, the rotational quantum number K was treated as active in evaluating the RRKM rates,⁴⁰ and the angular momenta were estimated from the average collision cross sections, i.e., $L = \mu v_{\text{rel}}(\sigma_{\text{col}}/\pi)^{1/2}$, where μ and v_{rel} are the reduced mass and relative velocity of collision, respectively. The complexes and TSs were described using scaled frequencies, polarizabilities, and moments of inertia from the *ab initio* calculations. Because the v_{axial} data are consistent with a complex-mediated mechanism only at the lowest range of E_{col} , we focus this discussion on the RRKM results for our lowest nominal E_{col} value of 0.1 eV.

The only significant decay channel for complex *A* is the isomerization to complex *B*, with negligible decay back to reactants, consistent with the observation that $\sigma_{\text{total}} \approx \sigma_{\text{col}}$ at low E_{col} . The RRKM calculation also predicts that the decay of complex *A* to CT products or to *trans*- $\text{CH}_2\text{CHCHO}^+$ via TS1 is negligible. For complex *B*, the dominant channel is the dissociation to HT products (89.5% at $E_{\text{col}}=0.1$ eV), with lower branching for isomerization back to complex *A* (8.8%), dissociation to PT products (1.7%), or isomerization

via TS3 to *trans*-CH₂CHCHO⁺ (<0.1%). Once formed, the *trans*-CH₂CHCHO⁺ complex does not convert back to complex *B* significantly, instead dissociating to HE products via TS4 (73%), or isomerizing over TS5 to CH₂CH₂CO⁺ (27%). Finally, any CH₂CH₂CO⁺ formed decays almost exclusively to HPT products.

There are two ways to compare the RRKM results with the experiment. If we assume that the v_{axial} distributions at low E_{col} are forward-backward symmetric because of complex rotation, this sets a lower limit on the required τ_{complex} of ~ 1.5 ps. The RRKM lifetime of complex *A* is significantly longer than those for complex *B*, *trans*-CH₂CH₂CHO⁺, and CH₂CH₂CO⁺, and thus it is the best candidate to account for the collision time. Complex *A* has a RRKM lifetime dropping from 3.5 ps at $E_{\text{col}}=0.1$ eV to ~ 1 ps at 0.5 eV. The lifetime is in the right range to account for the forward-backward symmetric v_{axial} distributions; however, this is only a necessary, but not sufficient condition for a complex-mediated mechanism.

A better test is to compare the experimental and RRKM branching ratios. The first failure is that RRKM predicts negligible CT branching over the entire E_{col} range, indicating that CT must be direct, even near threshold. It is possible that CT is decoupled from the other channels, where a complex mechanism might still be important. The real test is the branching among PT, HT, HE, and HPT. As discussed above, charge is delocalized in complex *B*, and it is reasonable to assume that it can dissociate to both the HT and PT charge states of the [C₂H₃+HCO]⁺ products. In the context of a statistical calculation, the only obvious way to treat this type of problem is to assume that the branching depends only on the state count at the orbiting TS in each channel, as in the usual case. This assumption is equivalent to assuming that the electronic degree of freedom is adiabatic, so that the electronic and nuclear degrees of freedom remain coupled during complex dissociation. With this assumption, complex *B* is calculated to decay almost exclusively to HT products at low E_{col} . For example, at $E_{\text{col}}=0.1$ eV, the net HT : PT : HPT : HE branching is predicted to be 96.3% : 1.9% : 0.5% : 1.3%. For comparison, the corresponding experimental branching is 16% : 21% : 54% : 9%.

Clearly the RRKM branching is in very poor agreement with the experiment; however, there are several points to consider before entirely dismissing a complex-mediated mechanism at low E_{col} . The biggest discrepancy is for the HPT channel, which has ~ 100 times greater branching than predicted. The RRKM branching to HPT is small because the calculated minimum-energy path is rather convoluted. The limiting step on that pathway is the decay of complex *B* to *trans*-CH₂CHCHO⁺ via the relatively tight TS3, which competes poorly with the dissociation to HT products. If there was an alternate route to HPT products, either direct or complex mediated, it might still be possible to account for the HT/PT/HE branching by a complex mechanism. The obvious alternative complex-mediated route to HPT products would be the transfer of hydrogen from HCO to C₂H₃ in complex *B*, directly generating HPT products. Such a process is unlikely to have a large activation energy, but we were unable to locate the transition state for this transformation, and are,

therefore, unable to include it in the RRKM calculation. In both the HPT pathway in Fig. 2 and that just described, the two H atoms are transferred sequentially, with or without additional rearrangements. It is also possible that concerted (i.e., near-simultaneous) H₂⁺ transfer might contribute to the HPT signal, either in a complex-mediated or direct mechanism. Direct production of H₂CCH₂⁺ by concerted transfer of one H to each carbon center in C₂H₂ could occur only in a very narrow range of H₂CO⁺-C₂H₂ orientations. There is no complex with the correct structure to promote such a mechanism in a complex-mediated mechanism, and the anisotropy of the long-range potential is far too weak to cause significant orientational steering in a direct mechanism. More likely, HPT might occur by concerted or rapid sequential H₂⁺ transfer to a single carbon center, initially forming CH₃CH⁺. Partial optimization of such a structure constrained to have C_{3v} geometry indicates that CH₃CH⁺+CO has an energy ~ 1 eV below the reactants, and in a full optimization, CH₃CH⁺ converges to H₂CCH₂⁺. The conclusion is that the reaction path H₂CO⁺+C₂H₂→CH₃CH⁺+CO→HPT products is energetically downhill, and therefore may be important.

If this or some other direct HPT production mechanism is invoked to rationalize the large HPT branching, there is still the question of whether the remaining HT, PT, and HE branching might be explained by a complex-mediated mechanism. It appears not. The RRKM-predicted HT: PT branching at $E_{\text{col}}=0.1$ eV is $\sim 98:2$, compared to the experimental 16:21 ratio, i.e., there is far more PT than predicted in a RRKM calculation based on state counts in the product channels.

The conclusion from the RRKM branching results is that most products are generated by direct reactions, even at the lowest E_{col} of this study. There is probably some complex-mediated reaction, as well, generating a fraction of the HT, PT, and HPT products. In addition, it seems likely that the minor HE channel requires mediation from a complex, because the required rearrangements would be difficult to imagine in a direct mechanism. At first glance it is surprising that the HE reaction never involves the loss of D in reaction with C₂D₂. In the proposed pathway: complex *A*→complex *B*→*trans*-CH₂CHCHO⁺→HE products, the only step where significant H/D exchange might be expected is in the *trans*-CH₂CHCHO⁺ intermediate. The RRKM calculations indicate that the *trans*-CH₂CHCHO⁺ lifetime is subpicosecond at low E_{col} , and thus are consistent with the absence of D elimination.

2. Branching as a probe of charge state "unmixing"

Probably the most interesting aspect of this reaction at low E_{col} is the competition among the major HT, PT, and HPT channels. At high E_{col} , the more facile HT and PT reactions dominate, and the HT/PT branching increasingly favors the lower energy HT charge state as E_{col} is reduced, as expected from a state count picture. Below $E_{\text{col}}\approx 0.5$ eV, both HT and PT show signs of competition from the rapidly growing HPT and HE channels. The HT cross section turns over and begins to decrease at low E_{col} , while over the same energy range the PT cross section continues to increase, but

with diminished slope. It is not surprising that HPT should compete with HT and PT, because HPT simply corresponds to the transfer of H^+ (or H) between the nascent HT (or PT) products. The growth of HPT as E_{col} is reduced, suggests that it becomes increasingly likely that this highly exoergic second atom transfer event occurs before the HT or PT products separate. It is quite surprising, however, that HPT competes unequally with the two channels, with the lower energy HT channel losing the most intensity. There is undoubtedly some effect of competition with the minor HE channel as well, given that $\sigma_{\text{total}} = \sigma_{\text{col}}$. Here too, however, it is not obvious why the competition would selectively deplete intensity from the more energetically favorable HT channel.

The selective competition of HPT (and HE) with HT tells us something about the mechanism controlling HT/PT branching. Recall that the charge is nearly equally partitioned between the C_2H_3 and HCO moieties in the product-like complex *B*, and presumably is also delocalized in other collision geometries where H/ H^+ transfer might occur. The question is at what point during product separation does the branching between the HT and PT charge states gets decided. Consider two possibilities. We might expect that the product charge states do not “unmix” until the $[C_2H_3-HCO]^+$ separation increases significantly beyond the equilibrium separation. In such a “late branching” scenario, it is difficult to see how the HPT channel could selectively compete with HT, because the second atom transfer event must occur at short C_2H_3-HCO separations where the HT and PT channels are still mixed. The same argument would apply to competition from the HE channel, because C–C bond formation clearly must occur at short C_2H_3-HCO separations.

The observation of selective competition with HT implies, therefore, that the HT-PT branching must be determined before there is significant product separation, so that HPT and HE can distinguish and compete selectively with HT and PT products. The difficulty for this “early branching” scenario is to explain how the HT and PT channels become distinguishable at small $[C_2H_3-HCO]^+$ separations, even though the charge states are almost certainly still mixed by the strong interaction potential. The key factor is the geometries of the C_2H_3 and HCO products, which are both quite different in the HT and PT channels (Fig. 2). The equilibrium HT geometry has linear HCO $^+$ and C_2H_3 with both carbon centers having CCH bond angles near 120° . The PT products have HCO bent at 125° , and $C_2H_3^+$ with one or both carbon centers having linear CCH geometry (depending on the $C_2H_3^+$ isomer). As a result, the potential surfaces for HT and PT products have displaced minima and cross along the coordinate corresponding to the combined HCO and CCH bond angle changes accompanying the electron transfer. The cuts along this “combined bending coordinate” through the HT and PT surfaces at infinite product separation are shown in the inset to Fig. 2, where the points are from B3LYP/6-311+G** single-point calculations, and the curves are simply schematic. For finite product separation, the crossing becomes avoided, and the resulting lower adiabatic surface has separate PT and HT valleys, displaced along the combined bending coordinate, and separated by a barrier. Finally, at very short $(HCO-C_2H_3)^+$ separations, as in complex *B*, the

interaction is evidently strong enough to eliminate the barrier, such that there is a single equilibrium structure with delocalized charge. (For this discussion, we will focus on the classical $C_2H_3^+$ isomer; however, the same arguments apply to the bridged isomer as well.)

Once the notion of early branching between HT and PT channels is accepted, it is not difficult to rationalize why the nascent HT products are more susceptible to competition from HPT and HE, than PT products. Both HPT and HE involve bond formation to the CH carbon center in the nascent H_2CCH product. In the HT charge state, this center has the correct sp^2 hybridization and bent geometry, and has an unpaired electron ready to make a bond. In the PT charge state, the $[H_2CCH]^+$ moiety is closed shell, and the carbon center of interest is sp hybridized and linear.

At high E_{col} , the separating HCO and C_2H_3 products have substantial vibrational excitation (E_{recoil} is only approximately half E_{avail}), and the system can probably vibrate across the barrier separating the HT and PT portions of the surface, until finally at large separations the products are trapped in one state or the other as the charge states unmix. At low E_{col} , it appears that the barrier separating the HT and PT channels is large enough to trap the system in one channel or the other, even at separations small enough to allow HPT and HE to deplete the nascent HT products preferentially. The vibrational effects discussed next provide additional insight into the factors controlling interchannel competition.

C. Vibrational effects

During the course of a collision, it is reasonable to expect that the reactants should lose memory of the initial vibrational state (as opposed to E_{vib}) relatively early, as interreactant interactions mix vibrational modes and interconvert energy among vibration, translation, and rotation. This consideration suggests that when mode-specific effects are observed, they reflect vibrational control at some critical point early on the reaction coordinate.^{6,41} The $H_2CO^+ + C_2H_2$ system reacts with unit efficiency ($\sigma_{\text{total}} = \sigma_{\text{col}}$) over a broad range of E_{col} , implying that the rate-limiting factor is simply the centrifugal barrier (i.e., angular momentum conservation). Such reactions are poor candidates for having significant vibrational effects: however, in this case, there are large effects on interchannel branching that are particularly helpful in sorting out competition effects. With the exception of the CT channel at high energies, the effects are largely proportional to vibrational energy. The lack of mode specificity suggests, not surprisingly, that control over product branching occurs after scrambling of the initial vibrational mode, but still early enough that the system retains some memory of the reactant vibrational energy.

1. Vibration as a probe of HT, PT, HPT, and HE dynamics

The vibrational effects shown in Fig. 8 provide additional insight into the competition that determines product branching. Note that HPT, HT, and HE are all inhibited by vibrational excitation, while PT is vibrationally enhanced in

the low E_{col} range where the competition occurs. This pattern is consistent with the idea of early branching between HT and PT, outlined above. In that scenario, the HT/PT branching occurs after atom transfer to generate $[\text{C}_2\text{H}_3\text{-HCO}]^+$, but before significant product separation. At that point, it is not unreasonable to expect the system to retain some memory of the initial H_2CO^+ vibrational energy, although atom transfer would certainly scramble the initial mode of excitation. Evidently, increasing H_2CO^+ vibration favors branching to the higher energy PT channel, at the expense of HT. The fact that HT, HPT, and HE all have similar, inhibitory vibrational dependence is consistent with the idea that the HPT and HE products form by subsequent intramolecular reactions of the nascent HT products, i.e., anything that suppresses HT also suppresses the subsequent reactions. Note that the vibrational suppression for the HPT and HE channels is stronger than that for HT itself. This result can be rationalized as follows. Increasing the reactant vibrational energy increases the available energy in the nascent $\text{C}_2\text{H}_3\text{-HCO}^+$ products, which should tend to shorten the time scale of product separation. Shorter time scale decreases the probability for the additional reaction steps needed for HPT or HE, thus amplifying the inhibition from vibrational excitation.

The fact that vibration enhances PT and inhibits the coupled HT/HPT/HE channels suggests that these vibrational effects result from the vibrational control of the HT/PT branching. The question remains why vibrational energy increases the PT/HT branching ratio at low E_{col} , particularly given the fact that for $E_{\text{col}} < \sim 0.4$ eV, increased E_{col} decreases the ratio. Within the early branching scenario, the most plausible mechanism is that H_2CO^+ vibrational excitation increases the vibrational energy of the nascent $(\text{HCO-C}_2\text{H}_3)^+$ products, as shown by the observation that vibrational excitation has little effect on the v_{axial} distributions. Given the nature of the exit channels (inset to Fig. 2), increased vibrational energy should increase the fraction of product flux that partitions into the higher energy PT exit channel, at the expense of HT signal. The contrary effect of collision energy on the HT/PT branching is consistent with the early branching scenario outlined above. The reason the HT cross section decreases at low E_{col} is competition with HPT and, to a lesser extent, with HE. Both HPT and HE are strongly suppressed by E_{col} , thus E_{col} decreases the PT/HT ratio.

2. Vibration as a probe of CT dynamics

In $\text{H}_2\text{CO}^+ + \text{C}_2\text{H}_2$ CT, neither reactant undergoes a large geometry change, thus none of the vibrational modes are expected to be strongly coupled to the CT reaction coordinate. We might expect, therefore, that the major effect of vibration is simply to provide additional energy, thus it is interesting to compare the effectiveness of different vibrational modes and collision energy in driving endothermic CT. From Fig. 7, where σ_{CT} is plotted against $E_{\text{col}} + E_{\text{vib}}$, it is apparent that vibrational excitation has effects similar to E_{col} in the threshold regime (E_{rot} is negligible, and the same for all states). In this E_{col} range, the v_{axial} distributions show that

the vibrational enhancement results from a vibration-induced increase in the range of impact parameters where CT is possible (see above).

To compare the cross sections more quantitatively, and to correct for broadening in the E_{col} distribution, we fit the experimental E_{col} dependence for each vibrational state, as discussed previously.^{7,42} A parametrized “true” $\sigma(E_{\text{col}})$ function is convoluted with the experimental primary beam and target velocity distributions, then adjusted until the result matches the experimental E_{col} dependence. For the true $\sigma(E_{\text{col}})$ function, we used a modified line-of-centers function discussed elsewhere,^{43,44}

$$\sigma(E_{\text{col}}) = \sigma_0 \frac{(E_{\text{col}} + E_{\text{vib}} + E_{\text{rot}} - E_0)^n}{E_{\text{col}}}, \quad (6)$$

where σ_0 is a normalization parameter, n controls the threshold curvature, E_0 is the thermodynamic threshold energy, and E_{col} , E_{vib} , and E_{rot} are the collision energy and total reactant vibrational and rotational energies. For the C_2H_2 target, the rotational and vibrational energies are thermal at room temperature. For H_2CO^+ , E_{vib} is the selected state energy and E_{rot} is negligible because our ions are produced by REMPI of a supersonic beam. The E_{col} distribution is determined from the measured primary beam velocity distribution and the thermal C_2H_2 velocity distribution.

The result is that within the fitting uncertainty, cross sections for all reactant vibrational states can be *adequately* fitted using the thermodynamic threshold energy and similar n parameters. These fits correspond to assuming that vibrational, rotational, and collision energies are equally effective in driving CT at threshold. We note, however, that the *best* fits are obtained if we treat E_{vib} as a fitting parameter, i.e., if we allow the possibility that vibrational energy may not be as effective as E_{col} in driving CT (E_{rot} is constant and too small to have a significant effect). For the low energy modes, the best fit E_{vib} is close to the actual state energy, implying that these low-frequency modes are equivalent to E_{col} at threshold. For the higher energy modes, the best fits are obtained for E_{vib} 15%–25% below the state energy, i.e., these modes drive CT with declining efficiency. Similar behavior was observed in CT of H_2CO^+ with OCS.⁷

This non-mode-specific vibrational enhancement is observed for E_{col} up to about 1.2 eV, but at that point there is a sharp transition to mode-specific vibrational inhibition, with ν_2^+ and ν_3^+ having the largest effects. At the same energy, there is also a decrease in the slope of σ_{CT} vs E_{col} , and the two factors together tend to suggest a change in the CT mechanism. The mechanism at low E_{col} clearly involves intimate collisions where E_{col} and E_{vib} can be converted to drive this endoergic process. At high E_{col} , the v_{axial} distributions are broad and backward peaked, indicating that CT occurs at increasingly large impact parameters, presumably reflecting the need to convert smaller fractions of E_{col} to drive CT. The observation of vibrational inhibition is unexpected, because added vibrational energy should reduce the fraction of E_{col} that must be converted to drive CT, allowing CT to occur in larger impact-parameter collisions. Inhibition suggests that some other factor is controlling the CT efficiency at high E_{col} .

The pattern of mode effects (Fig. 8) provides the necessary clue regarding this controlling factor. The pattern at high E_{col} is identical to those observed in CT of H_2CO^+ with ND_3 and C_2D_4 ,^{10,11} both in terms of the magnitude of the inhibitions and the mode dependence. In those systems, CT occurs by long-range electron hopping at inter-reactant separations considerably larger than the hard-sphere radius ($R_{\text{hard sphere}}$). As discussed in those papers, efficient long-range electron hopping requires that the initial and final states of the system be near resonant; however, this is usually not a problem for polyatomic species. In addition, because the long-range CT event is essentially an electronic transition, the efficiency of CT between a particular pair of initial and final states is influenced by the Franck-Condon factors connecting the states. For H_2CO^+ CT with ND_3 and C_2H_4 , the pattern of vibrational mode effects was shown to result from variations in the Franck-Condon factors for the neutralization of H_2CO^+ in different initial vibrational states.¹¹

The surprise is that the Franck-Condon factors appear to be important for $\text{H}_2\text{CO}^+ + \text{C}_2\text{H}_2$, where CT is endoergic and has a cross section an order of magnitude smaller than those in the ND_3 and C_2D_4 cases. The usual picture of endoergic CT is that a “hard” collision is needed to convert E_{col} to the internal energy that drives CT, and for such collisions, the Franck-Condon factors should be irrelevant. That is certainly the case here for CT for $E_{\text{col}} < 1.2$ eV, but at high E_{col} the backward-peaked v_{axial} distributions indicate that a substantial fraction of CT occurs in large b collisions. Apparently in such collisions, the interaction is weak enough to preserve the dependence on the Franck-Condon factors.

There are two issues raised by this conclusion. For the Franck-Condon factors to be important, it would appear that CT must be possible in collisions where the reactants never approach closer than $R_{\text{hard sphere}}$. A significant cross section for CT at impact parameters larger than $R_{\text{hard sphere}}$ seems inconsistent with the observation that $\sigma_{\text{total}} = \sigma_{\text{hard sphere}}$ at high E_{col} . Furthermore, if these CT collisions never reach $R_{\text{hard sphere}}$, it is not clear what mechanism is available to convert collision energy to drive CT. Analysis of nonreactive scattering provides additional insight into both issues.

D. Nonreactive scattering

Just as the PT and HT channels represent the two charge states of the $[\text{C}_2\text{H}_3 + \text{HCO}]^+$ products, CT is paired with the reactant charge state. The difference is that, for the HT and PT products, the equilibrium geometries are very different, while there is almost no geometry difference between the reactants and CT products. As a consequence, mixing of the CT and reactant charge states should be more facile. From this perspective, the CT mechanism might be described as follows: As the H_2CO^+ and C_2H_2 reactants approach, the interaction potential mixes the reactant and the CT charge states. In some fraction of collisions, no bond rearrangement reactions occur, and the $(\text{H}_2\text{CO} - \text{C}_2\text{H}_2)^+$ pair separate. As the separation increases, the charge state mixing breaks down, and the system ends up either as CT products or reactants. This branching back to the reactant charge state is omitted from σ_{total} , and if we could measure it, that would provide

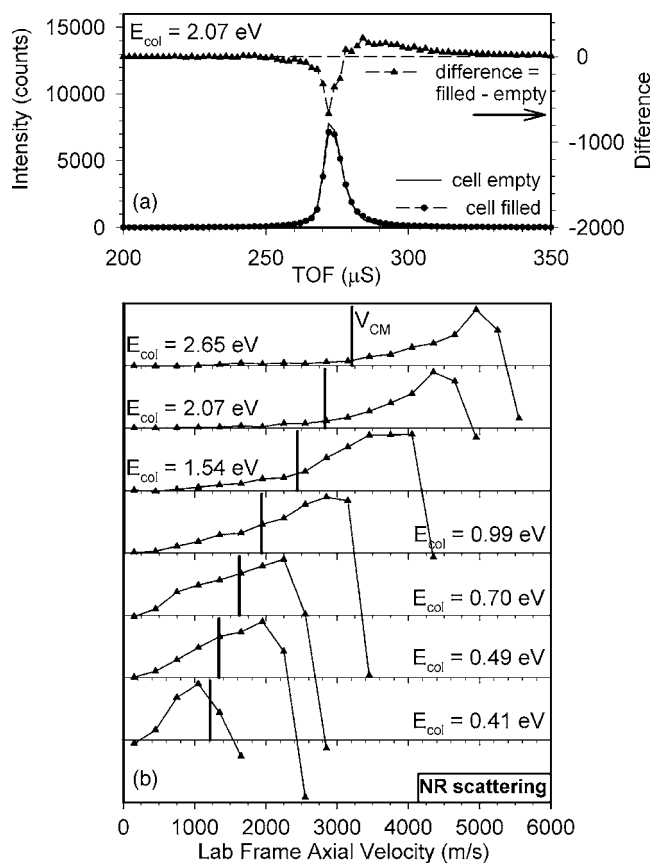


FIG. 9. (a) Upper frame: Time-of-flight spectra for the H_2CO^+ beam with the scattering cell filled and empty (left-hand scale), and the difference spectrum (right-hand scale). (b) Lower frame: Axial recoil velocity distributions for the nonreactively scattered H_2CO^+ . Heavy vertical line: $\langle V_{\text{c.m.}} \rangle$.

information about how far outside $R_{\text{hard sphere}}$ the system can be and still experience a significant collisional interaction. The usual problem is that nonreactive signal at the reactant ion mass is swamped by the reactant beam. With our pulsed, narrow energy spread beam, however, this signal can partially be recovered by the TOF analysis of the reactant ion signal.

The lower traces in Fig. 9(a) show the TOF distribution for the H_2CO^+ beam at $E_{\text{col}} = 2.07$ eV. The solid curve was measured with the scattering cell empty, and the points show the distribution when the cell was filled with C_2H_2 . The difference is plotted in the top trace. When the cell is empty, the H_2CO^+ beam has a sharp TOF distribution. Upon filling, the sharp peak is slightly attenuated and a feature appears on the long TOF side of the main peak. The attenuation results from a combination of reactive scattering removing H_2CO^+ from the beam and nonreactive scattering shifting H_2CO^+ intensity from the main peak to the long TOF feature. As can be seen from the intensities of the negative- and positive-going features in the difference spectrum, the reactive and nonreactive scattering cross sections are comparable at this collision energy.

The lower frame of the figure shows the v_{axial} distributions for nonreactively scattered H_2CO^+ at various collision energies. These are simply the TOF difference spectra converted to v_{axial} distributions. The negative peak from the primary beam attenuation is not shown, but its onset can be

seen as the negative-going excursions at high v_{axial} in each plot. It should be noted that these distributions represent only the fraction of the nonreactive scattering that slows the H_2CO^+ enough to allow it to be resolved from the primary beam by TOF analysis, i.e., only collisions with large net conversion of collision energy to internal energy of the products. For example, at $E_{\text{col}}=2.65$ eV, the peak in the v_{axial} distribution represents collisions where 1.5 eV of E_{col} was converted to internal energy. It is interesting that the v_{axial} distributions for nonreactive scattering are nearly mirror images of those for CT (Fig. 3), as would be expected from the discussion of charge state mixing at the beginning of this section. This result is probably not significant, however, because the high velocity cutoff of the nonreactive v_{axial} distributions is determined by our ability to resolve scattered H_2CO^+ from the primary beam.

More importantly, we can calculate the integral cross section for the resolvable nonreactive scattering σ_{nonreact} by simply integrating the positive portion of the v_{axial} distributions. It turns out that for $E_{\text{col}} > 1.0$ eV, σ_{nonreact} is $\sim 30 \text{ \AA}^2$, i.e., roughly equal to the total reaction cross section σ_{total} . Below 0.5 eV, σ_{nonreact} drops to near zero; however, we believe that the decrease is mostly from our decreasing ability to resolve the nonreactive signal. The important point is that the sum of σ_{total} and σ_{nonreact} at high E_{col} is $\sim 57 \text{ \AA}^2$ roughly double $\sigma_{\text{hard sphere}} (27.3 \text{ \AA}^2)$. A fraction of this "excess" cross section is attributable to the deflection by the long-range attractive potential, i.e., collisions with $b > R_{\text{hard sphere}}$ that are deflected such that a hard-sphere collision occurs. We estimated this fraction by running classical trajectories for scattering by an ion-induced dipole potential. For the E_{col} range between 1.5 and 2.65 eV, where $\sigma_{\text{hard sphere}}$ is relevant, entrance channel deflection can account for 15%–20% of the excess cross section.

The implication is that for high E_{col} , it is possible to have substantially inelastic collisions where the reactants never approach to $R_{\text{hard sphere}}$, and these are exactly the type of collision needed to account for the Franck-Condon factor dependence of CT at high E_{col} . The question is whether the $E_{\text{col}} \rightarrow E_{\text{internal}}$ conversion in such collisions is of the right type to drive CT or not. If the inelasticity in the nonreactive scattering was mainly rotational, we would not expect such collisions to have substantial CT probability. For ion-polar molecule collisions, the trajectories show substantial $E_{\text{col}} \rightarrow E_{\text{rot}}$ conversion at large impact parameters,^{10,11} because of the long-range torque applied to the dipole moment. C_2H_2 is nonpolar; however, the polarizability is highly anisotropic. At the B3LYP/6-311++G** level, α_{ZZ} is ~ 2.3 times greater than α_{XX} or α_{YY} . For a collision with an impact parameter $\sim 3.8 \text{ \AA}$ roughly in the middle of the range accounting for the excess cross section, the maximum torque resulting from this anisotropy is ~ 0.1 eV/rad. To estimate the likely amount of rotational excitation in such collisions, we ran a few trajectories at $E_{\text{col}}=2.5$ eV and $b=3.8 \text{ \AA}$, using the updating Hessian method of Bakken *et al.*⁴⁵ built into GAUSSIAN03 (Ref. 20) and the forces and the Hessians calculated at the B3LYP/6-31G** level. To avoid problems with multireference wave functions that might be significant in $(\text{H}_2\text{CO}-\text{C}_2\text{H}_2)^+$ collisions, we studied $\text{H}_2\text{NC}^+ + \text{C}_2\text{H}_2$ instead.

This ion has mass, size, and dipole moment similar to H_2CO^+ , but its ionization energy is low enough that significant contributions from $\text{H}_2\text{NC}-\text{C}_2\text{H}_2^+$ configurations can safely be discounted.

The result was that in trajectories where no hard collision occurred, the final rotational excitation was only < 0.1 eV. This result suggests that the large inelasticities measured in nonreactive scattering are not rotational, and therefore could reasonably be expected to drive CT. It is not clear what form the inelasticity takes. The trajectories show no signs of significant vibrational excitation, so it is not unlikely that we are observing some form of electronic inelasticity, presumably driven by some nonadiabaticity induced by the long-range potential. Unfortunately, the trajectory methods available at present cannot handle such situations, and we are unable to go beyond this speculation.

ACKNOWLEDGMENT

This work was supported by the National Science Foundation under Grant No. CHE-0110318.

- ¹M. Y. Amin, M. S. El Nawawy, B. G. Ateya, and A. Aiad, *Earth, Moon, Planets* **69**, 127 (1995).
- ²F. Arnold, D. Krankowsky, and K. H. Marien, *Nature (London)* **267**, 30 (1977).
- ³A. Dalgarno and J. H. Black, *Rep. Prog. Phys.* **39**, 573 (1976).
- ⁴J. Cernicharo, A. M. Heras, A. G. G. Tielens, J. R. Pardo, F. Herpin, M. Guelin, and L. B. F. M. Wayers, *Astrophys. J.* **546**, L123 (2001).
- ⁵G. J. Francis, P. F. Wilson, R. G. A. R. Maclagan, C. G. Freeman, M. Meot-Ner, and M. J. McEwan, *J. Phys. Chem. A* **108**, 7548 (2004).
- ⁶R. J. Green and S. L. Anderson, *Int. Rev. Phys. Chem.* **20**, 165 (2001).
- ⁷J. Liu, B. Van Devener, and S. L. Anderson, *J. Chem. Phys.* **117**, 8292 (2002).
- ⁸J. Liu, B. Van Devener, and S. L. Anderson, *J. Chem. Phys.* **119**, 200 (2003).
- ⁹J. Liu and S. L. Anderson, *J. Chem. Phys.* **120**, 8528 (2004).
- ¹⁰J. Liu, B. Van Devener, and S. L. Anderson, *J. Chem. Phys.* **121**, 11746 (2004).
- ¹¹J. Liu, B. Uselman, B. Van Devener, and S. L. Anderson, *J. Phys. Chem. A* **108**, 9945 (2004).
- ¹²Y.-H. Chiu, H. Fu, J.-T. Huang, and S. L. Anderson, *J. Chem. Phys.* **102**, 1199 (1995).
- ¹³Y.-H. Chiu, H. Fu, J.-T. Huang, and S. L. Anderson, *J. Chem. Phys.* **105**, 3089 (1996).
- ¹⁴Y.-H. Chiu, Ph.D. thesis, State University of New York at Stony Brook, 1996.
- ¹⁵J. Liu, B. Van Devener, and S. L. Anderson, *J. Chem. Phys.* **116**, 5530 (2002).
- ¹⁶R. Spence and W. Wild, *J. Chem. Soc.* 1935, 338.
- ¹⁷F. S. Dainton, K. J. Ivin, and D. A. G. Walmsley, *Trans. Faraday Soc.* **55**, 61 (1959).
- ¹⁸J. Liu, H.-T. Kim, and S. L. Anderson, *J. Chem. Phys.* **114**, 9797 (2001).
- ¹⁹D. Gerlich, *Adv. Chem. Phys.* **82**, 1 (1992).
- ²⁰M. J. Frisch, G. W. Trucks, H. B. Schlegel *et al.*, GAUSSIAN 03 (Gaussian, Inc., Pittsburgh, PA, 2003).
- ²¹J. B. Foresman and A. Frisch, *Exploring Chemistry with Electronic Structure Methods*, 2nd ed. (Gaussian, Pittsburgh, 1993).
- ²²L. Zhu and W. L. Hase, *A general RRKM program (QCPE 644)* (Chemistry Department, University of Indiana, Bloomington, 1993).
- ²³S. G. Lias, J. E. Bartmess, J. F. Liebman, J. L. Holmes, R. D. Levin, and W. G. Mallard, *J. Phys. Chem. Ref. Data Suppl.* **17** (1) (1988).
- ²⁴S. G. Lias, in *NIST Standard Reference Database Number 69*, edited by P. J. Linstrom and W. G. Mallard (National Institute of Standards and Technology, Gaithersburg, MD, 2003) <http://webbook.nist.gov>
- ²⁵D. K. Bohme, in *Interactions between Ions and Molecules*, edited by P. Ausloos (Plenum, New York, 1975), p. 489.
- ²⁶J. L. Holmes and F. P. Lossing, *Int. J. Mass. Spectrom.* **58**, 113 (1984).

- ²⁷ F. P. Lossing and J. L. Holmes, *J. Am. Chem. Soc.* **106**, 6917 (1984).
- ²⁸ Y. Li and T. Baer, *Int. J. Mass. Spectrom.* **2181**, 19 (2002).
- ²⁹ M. L. McKee and L. Radom, *Org. Mass Spectrom.* **28**, 1238 (1993).
- ³⁰ F. Turecek, D. E. Drinkwater, and F. W. McLafferty, *J. Am. Chem. Soc.* **113**, 5950 (1991).
- ³¹ F. Turecek, D. E. Drinkwater, and F. W. McLafferty, *J. Am. Chem. Soc.* **113**, 5958 (1991).
- ³² G. Bouchoux, *J. Mol. Struct.: THEOCHEM* **151**, 107 (1987).
- ³³ E. D. Glendening, A. E. Reed, J. E. Carpenter, and F. Weinhold, *NBO* version 3.1.
- ³⁴ J. C. Traeger, C. E. Hudson, and D. J. McAdoo, *Org. Mass Spectrom.* **24**, 230 (1989).
- ³⁵ J. L. Holmes, J. K. Terlouw, and P. C. Burgers, *Org. Mass Spectrom.* **15**, 140 (1980).
- ³⁶ M. S. Child, *Molecular Collision Theory* (Academic, London, 1974).
- ³⁷ R. D. Levine and R. B. Bernstein, *Molecular Reaction Dynamics and Chemical Reactivity* (Oxford University Press, New York, 1987).
- ³⁸ G. A. Fisk, J. D. McDonald, and D. R. Herschbach, *Discuss. Faraday Soc.* **44**, 228 (1967).
- ³⁹ M. T. Rodgers, K. M. Ervin, and P. B. Armentrout, *J. Chem. Phys.* **106**, 4499 (1997).
- ⁴⁰ L. Zhu and W. L. Hase, *Chem. Phys. Lett.* **175**, 117 (1990).
- ⁴¹ J. Liu and S. L. Anderson, *Int. J. Mass. Spectrom.* **241**, 173 (2005).
- ⁴² H.-T. Kim, J. Liu, and S. L. Anderson, *J. Phys. Chem. A* **106**, 9798 (2002).
- ⁴³ M. B. Sowa-Resat, P. A. Hintz, and S. L. Anderson, *J. Phys. Chem.* **99**, 10736 (1995).
- ⁴⁴ P. B. Armentrout, *Int. J. Mass. Spectrom.* **200**, 219 (2000).
- ⁴⁵ V. Bakken, J. M. Millam, and H. B. Schlegel, *J. Chem. Phys.* **111**, 8773 (1999).